Energy Conversion and Management 270 (2022) 116258

Contents lists available at ScienceDirect

Energy Conversion and Management

journal homepage: www.elsevier.com/locate/enconman

Optimal design of annular thermoelectric generator with twisted tape for performance enhancement

WenChao Zhu [a,b], Aoqi Xu [a], Wenlong Yang [a], Binyu Xiong [a], Changjun Xie [a,b,*], Yang Li [a], Lamei Xu [a], Ying Shi [a], Wei Lin [a]

[a] School of Automation, Wuhan University of Technology, Wuhan 430070, China
[b] Hubei Key Laboratory of Advanced Technology for Automotive Components, Wuhan University of Technology, Wuhan 430070, China

ARTICLE INFO

Keywords:
Waste heat recovery
Annular thermoelectric generator
Twisted tape
Fluid-thermal-electric model
Multi-objective optimization

ABSTRACT

The adaptation of annular thermoelectric generator (ATEG) to cylindrical heat sources exhibits a better performance compared to widely studied flat plate type thermoelectric generator (FTEG). To enhance heat transfer and improve the overall performance, a novel structure of the heat exchanger of the twisted-tape annular thermoelectric generator (TT-ATEG) is proposed in this paper. A three-dimensional finite element model of TT-ATEG is established for the first time. The net power gain coefficient and the efficiency gain coefficient are defined to quantify the performance of TT-ATEG, and the gain effects of the length, twist ratio and radius of the twisted tape are analyzed respectively. To maximize the comprehensive performance of TT-ATEG, the optimal weighting factor of net power and efficiency are determined, and the full-parameter optimization of the twisted tape is completed. The results reveal that the optimal performance of TT-ATEG is obtained if the weight ratio of net power and conversion efficiency is 1:4. In our case study, dimensionless factors radius ratio R_r, length ratio L_r and twist ratio of the twisted tape are 0.714, 0.479 and 136.84 respectively. Compared with the ATEG without twisted tape, the net power and efficiency are improved by 10.41% and 22.51%, respectively. The results demonstrate that the novel design of TT-ATEG could accelerate the heat transfer effectively and enhance the overall performance.

1. Introduction

1.1. Literature review

With the increasing global energy crisis and the excessive carbon emissions, research on green and clean energy has become hot research topic today [1,2]. As an important research filed, a promising technology, thermoelectric generators (TEG), can convert thermal energy into electricity have attracted much attention due to the merits of friendly-to-environmental, noise free feature, good reliability and ect. It can not only recover a large amount of low-grade waste heat generated in industry and social life, but also can be coupled with geothermal power generation and solar power generation modules to generate electricity, which is crucial for improving energy utilization.

TEG usually consists of a heat exchanger and many thermocouples [3]. These thermocouples are usually connected in a fashion of thermal parallel and electrical series to generate high rating power for actual electricity use [4,5]. But the advance of large-scale TEGs commercialization process has been hindered due to the low thermoelectric efficiency [6]. The thermoelectric efficiency is calculated as follows [7]:

$$\eta_{\text{power}} = \eta_c \frac{\sqrt{1+Z\overline{T}}-1}{\sqrt{1+Z\overline{T}}+T_C/T_H} \tag{1}$$

where $\eta_c=(T_H - TC)/T_H$ is the Carnot efficiency, $\overline{T} = (T_H + TC)/2$ is the average temperature of the cold and hot ends, and the ZT is the figure of merit. From Equation (1), it can be seen that there are two main approaches to improve the performance of TEG: 1) Increasing the value of ZT or 2) Increasing the working temperature difference of ATEG. The ZT is mainly determined by the material properties, which is widely studied by researchers in the materials field. Zhang et al. [8] studied the material system of multiphase nanostructures, and the ZT value of the sample reached 1.83 at 773 K. Gerda Rogl et al. [9] prepared high ZT value of skutterudites from commercial powders by cold pressing and high

* Corresponding author at: School of Automation, Wuhan University of Technology, Wuhan 430070, China.
E-mail address: jackxie@whut.edu.cn (C. Xie).

https://doi.org/10.1016/j.enconman.2022.116258
Received 18 May 2022; Received in revised form 15 September 2022; Accepted 16 September 2022
Available online 26 September 2022

pressure torsion, and the *ZT* value reached to 2.1 at 850 K. Besides, many researchers used combined thermoelectric materials to increase the efficiency within wide temperature ranges, such as the proposed segmented TEG [10,11] or two-stage TEG [12,13] to maximize the *ZT* value by using different materials to improve the performance.

In the context of automotive exhaust heat recovery, the automotive exhaust gas temperature defines the operating temperature range of the hot source, resulting in a nearly deterministic selection of thermoelectric materials [14]. Therefore, it is a very promising way to improve the overall performance of TEG by heat transfer enhancement, which could raise the temperature difference between the two sides of the TEG [15].

Scholars usually achieve the purpose of enhancing heat transfer by improving the structure of the heat exchanger. Luo et al. [16] proposed a convergent heat exchanger with an appropriate tilt angle, which can effectively raise the TEG's hot end temperature and result in an increase in net power.

Yang et al. [17] designed an annular thermoelectric generator (ATEG) with a concentric annular heat exchanger, leading to an increase of the total output power of the ATEG while avoiding excessive back pressure. Wang et al. [18] used metal foams with high porosity in heat exchangers for TEG system, which could effectively improve the heat transfer performance of heat exchangers which could significantly improve heat transfer performance while minimizing the adverse effect of flow pressure drop on system performance. Kim et al. [19] used fin structure to enhance the heat transfer performance of an automotive TEG heat exchanger. They discovered that increasing the number and thickness of fins raises the temperature on the hot side of the TEG, while progressively increasing the pressure drop along the pipe. Lu et al. [20] increased the total power and net power output by arranging a lot of heat transfer enhancing elements of the heat exchanger.

However, most of the heat transfer enhancement is usually accompanied by an increase in pressure drop, resulting in an increase in backpressure power loss. In the process of exhaust heat recovery, excessive backpressure power loss would reduce the overall output power of the engine [21]. This may have negative impacts, leading to a reduction in the overall energy utilization of the system.

To quantify the effect of enhanced heat transfer measures on TEG output performance, the effect of total output power and backpressure power loss must be considered comprehensively. Wang et al. [14] proposed a performance evaluation index for the TEG system, but it cannot intuitively reflect the balance between the increased power generation and the extra backpressure power loss. Borcuch et al. [22] used net power to evaluate the improvement of TEG thermoelectric performance with different heat transfer enhancement structures. Yang et al. [23] established the concept of net power ratio to assess ATEG performance, and completed the design of ATEG with the guidance of the highest net power. Therefore, a proper evaluation index is needed in this paper to reflect the heat transfer enhancement and achieve the objectives of highest system efficiency and net power.

1.2. Gap and contribution

In recent years, flat-plate thermoelectric generator (FTEG) has been extensively studied. However, it cannot fit the exhaust pipe of the automobiles, which would cause additional contact thermal resistance and thermal energy loss. Shen et al. [24] propose ATEG that can be applied to cylindrical heat sources and demonstrate the superiority of the structure. Zhang et al. [25] examined the output power and conversion efficiency of FTEG and ATEG at varied velocities, temperatures and convection coefficients in a cylindrical heat source environment, and concluded that the ATEG outperformed the FTEG. Inspired by this, ATEG has gradually attracted the attention of scholars. ATEG has also demonstrate its applications in flexible micro-light-emitting diodes [26], annular solar thermoelectric generators [27] and LNG cold energy recovery [28], etc.

ATEG is a new research hotspot in the field of thermoelectricity. However, exploration and research on its enhanced heat transfer method has not been fully carried out. Overcomplicated modification of the heat exchanger will not only increase the retrofit cost, but also increase the exhaust backpressure, resulting in a decrease in the net power of the TEG. Limited by the low power generation efficiency and the initial cost of TEG, it has become an urgent issue to explore a simple, low-cost and practical way to enhance heat transfer for ATEG.

Twisted tapes are relatively simple to manufacture, low in cost, easy to install, and very suitable for technical updates of old heat exchangers. Some researchers have already demonstrated the advantages of twisted tapes in the field of heat transfer [29–31]. When twisted tapes are applied to TEGs, it is a great challenge to characterize and optimize the design with the guidance of thermoelectric system's traditional indices.

In this paper, the twisted tapes are applied to ATEG for the first time, and the impact of its critical parameters on thermoelectric output performance is explored. The TT-ATEG's comprehensive performance optimization index is proposed, and the optimal parameter configuration of the twisted tapes is completed by multi-objective optimization algorithm. The paper gives twisted tapes a new application scenario and demonstrates potential utility of TT-ATEG. The main contributions and innovations are as follows.

1) A three-dimensional finite element model incorporating twisted tapes and ATEG is established for the first time in Comsol. The analysis of TT-ATEG performance is conducted under the coupling of multiple physical fields of fluid-thermal-electricity.
2) Considering the backpressure power loss, the sensitivity of key parameters such as length, radius and twist ratio of twisted tape are analyzed on net power and efficiency.
3) The TT-ATEG performance optimization index is proposed, and the output performance is maximized by optimizing the parameters of the twisted tapes through joint multi-objective optimization in Matlab and Comsol.

The paper is structured as follows, the Section 2 introduces the TT-ATEG structure and modeling method, and the Section 3 verifies the accuracy of the model. Section 4 conducts a comprehensive analysis of TT-ATEG which achieves the optimal system performance through multi-objective optimization algorithm. Section 5 summarizes the main conclusions.

2. Modeling of TT-ATEG

2.1. Structure of TT-ATEG

Considering the coupling effects of the fluid-thermal-electrical multiphysics, a three-dimensional numerical model of TT-ATEG is established for cylindrical heat sources such as automobile exhaust pipes. The schematic view of the TT-ATEG is shown in Fig. 1(a), which consists of heat exchanger with a twisted tape and 72 pairs of annular thermoelectric couples (ATEC). The heat exchanger carries hot air inside and cooling water channel outside, with ATECs in between.

TT-ATEG has 6 rings and each ring contains 12 pairs of ATECs. The structural diagram of ATEC is shown in Fig. 1(b), which consists of a P-type and *N*-type thermelectric leg, conductive copper sheets, and ceramic sheets. h and w indicate the height and width of the P/*N*-type thermoelectric leg, and $\theta_{P/N}$ and θ_{in} indicate the angle of the P/*N*-type thermoelectric leg and the angle of the gap between the two thermoelectric legs. This paper considers the temperature dependence of thermoelectric materials, whose physical properties (Seebeck coefficient, electrical resistivity, thermal conductivity) are varying with respect to the temperature. The specific geometric parameters and physical properties of the ATEC is listed in Table 1.

The axial section view of the twisted tape inside the heat exchanger is shown in Fig. 1(c). The length and radius of the heat exchanger express as L_{ex} and R_{ex} respectively, and the twisted tape is fixed at $L_{ex}/2$. The

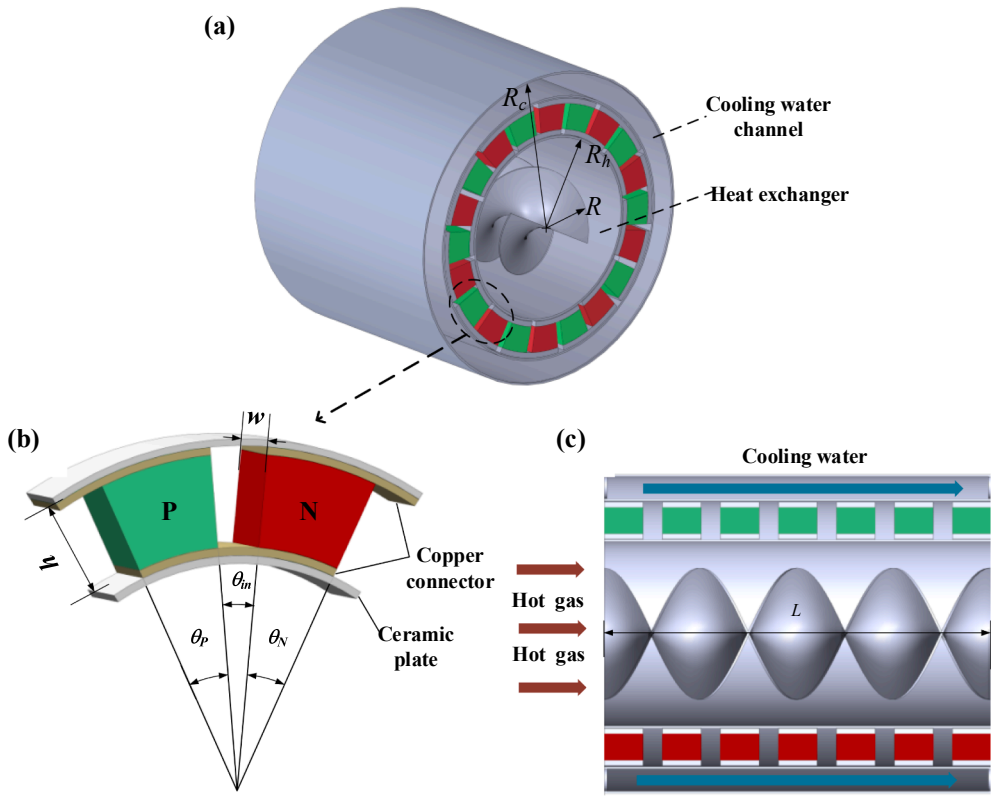

Fig. 1. Schematic view of the TT-ATEG: (a) overall structure, (b) 3D view of an annular thermoelectric couple, and (c) axial section view.

Table 1
Main geometric parameters and physical properties of ATEC [32].

Parameters	Description	Value	Unit
$l/w/h$	Dimensions of PN couple (length/width/height)	0.005/0.012/0.005	m
θ_{in}	The angle between P(N)-type leg	5	deg
$\theta_{P/N}$	The angle of P(N)-type leg	5	deg
λ_p	Thermal conductivity of p-type thermoelectric legs	$3.04\times10^{-10}T^4-3.89\times10^{-7}T^3+1.99588\times10^{-4}T^2-5.118914\times10^{-2}T+6.9245746$	W/(m·K)
α_p	Seebeck coefficient of p-type thermoelectric legs	$-4.88\times10^{-16}T^4+9.17\times10^{-13}T^3-3.18\times10^{-9}T^2+2.3184\times10^{-6}T-2.55904\times10^{-4}$	V/K
σ_p	Electrical resistivity of p-type thermoelectric legs	$-1.9\times10^{-16}T^4+3.47\times10^{-13}T^3-3.32\times10^{-10}T^2+1.96768\times10^{-7}T-2.849603\times10^{-5}$	Ω·m
λ_n	Thermal conductivity of *n*-type thermoelectric legs	$-7.6\times10^{-11}T^4+1.12\times10^{-7}T^3-5.162\times10^{-5}T^2+6.514882\times10^{-3}T+1.425785$	W/(m·K)
α_n	Seebeck coefficient of *n*-type thermoelectric legs	$1.36\times10^{-15}T^4-2.5\times10^{-12}T^3+2.94\times10^{-9}T^2-1.5018\times10^{-6}T+7.42322\times10^{-5}$	V/K
σ_n	Electrical resistivity of *n*-type thermoelectric legs	$-2.98\times10^{-16}T^4+4.92\times10^{-13}T^3-3.82\times10^{-10}T^2+1.79153\times10^{-7}T-1.95922\times10^{-5}$	Ω·m

twisted tape is constructed using parametric surfaces in Comsol, and the parametric equation of the twisted tape is:

$$\begin{cases} x = L \\ y = R\times\cos(aa\times L) \\ z = R\times\sin(aa\times L) \end{cases} \quad (2)$$

The geometry of the twisted tape is configured by three parameters, radius R, length L, and twist ratios aa. The geometric parameters of the heat exchanger and the twisted tape are shown in Table 2.

The hot exhaust gas of temperature, T_h, and mass flow rate, m_h, flows into the entrance of the heat exchanger, which is the heat source of the TT-ATEG. A part of the heat energy of the gas is transferred to the hot end of the ATEC through convection heat transfer, and a larger part is released through exhaust pipe. To improve energy conversion efficiency, the twisted tape is added to strengthen the heat transfer, which is a simple and practical structure twisted by a thin sheet. It enables the hot gas to produce spiral flow along the tie, increasing the heat transfer area and speeding up the transfer of heat between the fluid and the pipe wall. So as to maintain the working temperature difference of ATEG, cooling water is cycling at the cold side for cooling. The temperature of the

Table 2
Dimensional parameters of heat exchanger and twisted tape.

Parameters	Description	Value	Unit
L_{ex}	Length of Heat exchanger	0.097	m
R_{ex}	Heat exchanger radius	0.037	m
δ_{ex}	Heat exchanger tube wall thickness	0.001	m
L	Length of twisted tape	0.097	m
R	Radius of twisted tape	0.02	m
aa	Twist ratios of twisted tape	100	/
δ_{cu}	Thickness of copper connector	0.001	m
δ_{cer}	Thickness of ceramic plate	0.002	m

cooling water is T_c, the mass flow rate is m_c, and the flow direction is the same as the hot gas.

Due to the Seebeck effect, part of the thermal energy absorbed by the thermocouple is converted into electrical energy. The cold end fluid dissipates the rest of the energy. In order to ensure that the TEG can obtain the maximum output power, the load resistance R_l is equal to the internal resistance. The hot and cold fluid properties and boundary condition settings is shown in Table 3.

2.2. Governing equation

In this section, Comsol is used to create a three-dimensional numerical model of the TT-ATEG, which involved fluid-thermal-electric multiphysics, Fluids and solids follow different laws of energy conservation, so the control equations are stated in two parts. The water and air in cold and hot sides of the heat exchanger are fluids and follow the conservation rule of mass, momentum and energy [33,34]:

$$\nabla\cdot(v) = 0 \tag{3}$$

$$\nabla\cdot(vv) = -\frac{1}{\rho}\nabla p + \nabla\cdot(\mu\nabla v) \tag{4}$$

$$\nabla\cdot(\lambda\nabla T) = \rho c v\cdot\nabla T \tag{5}$$

where, v is the flow velocity, ρ is the fluid density, P is the fluid pressure, μ is the dynamic viscosity, λ is the thermal conductivity, c is the specific heat capacity.

Considering the temperature and Reynolds number, the gas flow inside the heat exchanger is turbulent. Apply the standard k-ε function to obtain the turbulent kinetic energy and energy dissipation of the fluid in the pipe. Its transport equations are as follows:

$$\frac{\partial}{\partial t}(\rho k) + \frac{\partial}{\partial x_i}(\rho k u_i) = \frac{\partial}{\partial x_j}\left[\left(\mu + \frac{\mu_t}{\sigma_k}\right)\frac{\partial k}{\partial x_j}\right] + G_k + G_b - \rho\varepsilon - Y_M \tag{6}$$

$$\frac{\partial}{\partial t}(\rho \varepsilon) + \frac{\partial}{\partial x_i}(\rho \varepsilon u_i) = \frac{\partial}{\partial x_j}\left[\left(\mu + \frac{\mu_t}{\sigma_\varepsilon}\right)\frac{\partial \varepsilon}{\partial x_j}\right] + C_{1\varepsilon}\frac{\varepsilon}{k}(G_k + C_{3\varepsilon}G_b) - C_{2\varepsilon}\rho\frac{\varepsilon^2}{k} \tag{7}$$

where G_k is the generation term of the turbulent kinetic energy k caused by the average velocity gradient, G_b is the generation term of the k caused by the buoyancy, and $C_{1\varepsilon}$,$C_{2\varepsilon}$,$C_{3\varepsilon}$ are empirical constants. For more details about Eqs. (5) and (6) refer to [35].

The above equations have modeled the fluid regions (air and water). The solid region follows a simple energy balance.

$$\nabla\cdot(\lambda\nabla T) = 0 \tag{8}$$

The heat flow's steady-state governing equation is written as [36]:

$$\nabla\cdot q = \dot{q} \tag{9}$$

where q and $\dot{q}$ denote the heat flux vector and the heat generation rate, respectively.

The electric field intensity vector E is defined as:

$$E = -\nabla\varphi + \alpha\nabla T \tag{10}$$

where φ is the electric potential, and $\alpha\nabla T$ is the Seebeck electric motive force.

The current density vector J can be expressed as:

$$J = \sigma E \tag{11}$$

where σ is the conductivity. Furthermore, since the current is continuous, the governing equation of electric charge is as follows [37]:

$$\nabla\cdot J = 0 \tag{12}$$

Based on Eqs. (9)-(12), the thermoelectric coupling equation can be derived as:

$$\begin{cases} q = \alpha T J - \lambda\nabla T \\ J = \sigma(E - \alpha\nabla T) = -\sigma(\nabla\phi_e + \alpha\nabla T) \end{cases} \tag{13}$$

2.3. Parameter definition

The heat absorbed by the hot end of the TEG system (Q_h) mainly comes from the convective heat transfer of the air in the heat exchanger (Q_{conv}), so it can be assumed that:

$$Q_h = Q_{\text{conv}} \tag{14}$$

When the hot gas flows through the heat exchanger, the heat absorbed by the hot end can be expressed as [38]:

$$Q_h = \dot{m}_h C_h (T_i - T_o) \tag{15}$$

where T_i and T_o represent the inlet and outlet temperatures of the hot gas.

The average value of heat absorbed by hot gas due to convective heat transfer is:

$$Q_{\text{conv}} = hA(T_{\text{w}} - T_{\text{b}}) \tag{16}$$

where A is the inner surface area of the heat exchanger, T_w is the average temperature of the inner wall, and T_b is the average hot gas temperature.

The average heat transfer coefficient h can be determined by Eqs. (13)-(15):

$$h = \left(\dot{m}_h C_h (T_i - T_o)\right) \Big/ \mathrm{A}\left(\widetilde{T}_{\text{w}} - T_{\text{b}}\right) \tag{17}$$

The Nusselt number can be calculated as [39]:

$$Nu = \frac{hD}{k} \tag{18}$$

where D is the hydraulic diameter, and k is the thermal conductivity.

The coefficient of friction is defined as follows [40]:

$$f = \frac{\Delta P}{\left(\frac{1}{2}\rho v_{in}^2\right)\left(\frac{L}{D}\right)} \tag{19}$$

where v_{in} is the average velocity of the fluid inlet, ΔP is the pressure drop, which can be calculated by post-processing.

The twisted tape would increase the frictional resistance along the way, and the backpressure power loss can be calculated as:

$$P_{loss} = \dot{V}_h \Delta P \tag{20}$$

where V_h is the hot gas volumetric flow rate. The TEG system's output power is calculated by:

$$P_{out} = I^2 R_L \tag{21}$$

where I is the output current of the TT-ATEG, R_L is the load resistance.

Table 3
Parameters of hot and cold fluid properties and boundary condition.

Parameters	Description	Value	Unit
R_h	Hot gas channel radius	0.037	m
R_c	Cooling water channel radius	0.040	m
T_h	Hot gas inlet temperature	673.15	K
T_c	Cooling water inlet temperature	293.15	K
m_h	Mass flow rate of hot gas	30	g/s
m_c	Mass flow rate of cooling water	300	g/s
ρ_h	Fluid density of hot gas	0.52	kg/m^3
ρ_c	Fluid density of cooling water	998.2	kg/m^3
μ_h	Dynamic viscosity of hot gas	3.25×10^{-5}	Pa·s
μ_c	Dynamic viscosity of cooling water	100.93×10^{-5}	Pa·s
R_L	Load resistance	0.1192	Ω

Net power P_{net} and conversion efficiency are defined as:

$$P_{net} = P_{out} - P_{loss} \tag{22}$$

$$\eta = \frac{P_{out}}{Q_h} \tag{23}$$

2.4. Multi-objective optimization method

The proposed model and genetic algorithm are combined to optimize the output performance of TT-ATEG by configuring the parameter of the twisted tape. The livelink in Comsol provides a bridge for the data interaction between the Comsol and Matlab [24]. The genetic algorithm is a method to solve problems based on natural selection and biological evolution process. The genetic algorithm randomly selects a number of individuals from the current population as parents at each step and generates the next generation of subpopulations through selection, crossover, and mutation. The population evolves towards the optimal solution after several generations. In this paper, the genetic algorithm is realized by the toolbox in Matlab, which integrates various mature genetic operators and various improved genetic algorithms.

The process of joint optimization simulation is as follows: 1) Run MATLAB genetic algorithm to generate design variables (radius, length and twist ratio) and set key parameters for genetic optimization; 2) Complete the parametric modeling and calculation of TT-ATEG in Comsol; 3) Based on the calculation results of Comsol, Matlab calculates the objective function, and completes the parameter optimization through the genetic algorithm. The joint optimization simulation steps of the two software are shown in Fig. 2.

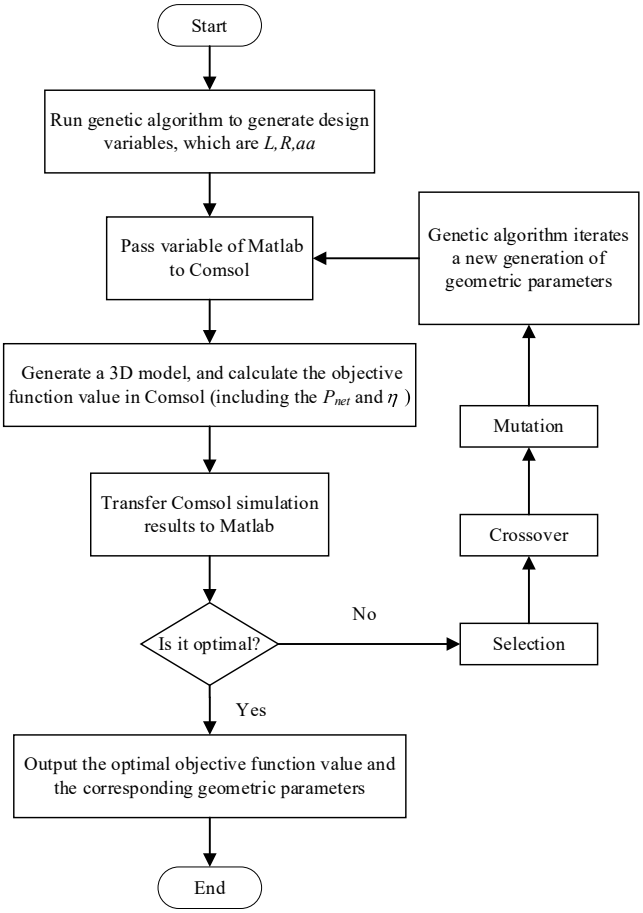

Fig. 2. Flowchart of Comsol with Matlab optimization.

3. Model validation

Due to the long manufacturing processing and high investment cost, current study on ATEGs are mainly based on simulation, and there are no available experimental data yet. To verify the model more rigorously, the verification process is divided into two parts. We first validate the modeling method's correctness by comparing it with FTEG experimental data [41], and then compare with the ATEG simulation data [23] to validate the accuracy of our model results.

3.1. Validation of modeling method

According to the researcher who proposed ATEG, this structure can be regarded as a special case of FTEG. When the radius of the annular thermoelectric couple is large enough, the curvature corresponding to the inner arc circular of the thermocouple is small, and the annular thermoelectric couples can be regarded as flat thermoelectric couples. Therefore, ATEG could be verified by the experimental data of FTEG. We use the data of FTEG in the Ref [41] for verification. They studied the positive effects brought by the spiral inserts in FTEG. The experiment was conducted on a FTEG composed of 40 commercial thermoelectric modules, with the sizes of 30 mm × 30 mm × 4.8 mm. The spiral inserts are made of 0.51 mm thick copper sheets twisted every 10 cm along their length direction.

To verify the proposed modeling method, we set the same model parameters (FTEG) and boundary conditions in Comsol according to the experimental conditions.

A comparison of the output power P_{out} and voltage U_{out} between the simulation results and experimental data in Fig. 3. It shows that the output power and voltage calculated by the Comsol are generally coherent with the experimental data, but slightly higher than the experimental data. The maximum deviation of U_{out} is 4.77 %, and the maximum deviation of P_{out} is 8.52 %. The reasons for this may account for simplifying assumptions in numerical model. For example, the outer surface of the cold end is set as an ideal adiabatic condition, but there would be a certain amount of heat loss in the actual experiment. Additionally, the walls of the heat exchanger pipes are set to be smooth in the simulation, but that is an ideal case in the actual situation. Therefore, these discrepancies are within a reasonable range and the modeling method is effective.

3.2. ATEG model results validation

In Ref [23], an similar ATEG system is proposed to recover the waste

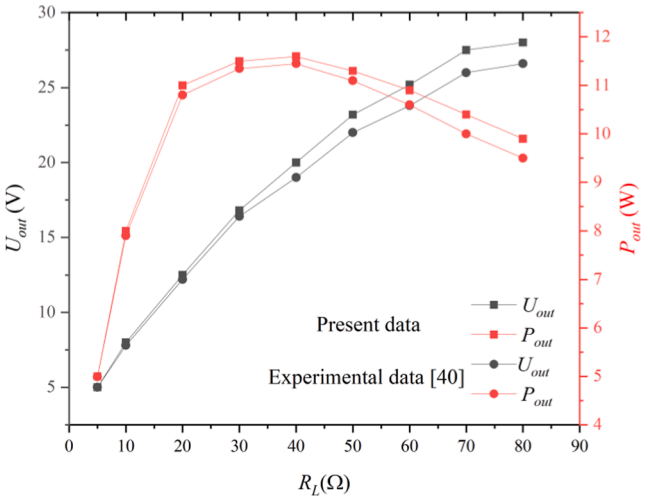

Fig. 3. Comparison of output voltage and output power between present data and experimental data [40].

heat of automobile. Yang et al. built a one-dimensional thermal resistance model with constant physical properties in Matlab. For validation, we set same model parameters with Ref. [23] and obtain the results under the conditions of $T_{cin} = 25$ ℃, $m_{cin} = 0.025$ g/s. $T_{fin} = 350$ ℃–650 ℃, $m_{fin} = 30$ g/s. Fig. 4 shows the comparison of net power under different T_{fin}. The deviation would increase with the increase temperature of the heat end and the maximum deviation is 9.85 %. This is because the three-dimensional finite element model set up in this paper has made many improvements based on the thermal resistance model. Specifically, model built by Comsol fully considers the influence of the interconnection of the flow field and the temperature field. The fluid properties are changed by the influence of temperature. In return, the fluid would also affect the surface temperature of the thermocouple. The thermal resistance model built by Matlab assumes that the fluid temperature changes linearly along the flow direction, while the temperature of the ATEC may not change in that way. Moreover, thermoelectric materials set in our model have variable properties according to the temperature, which is similar to the actual situation. While the properties of thermoelectric materials were set as fixed values in Ref. [23].

In summary, the ATEC model in this paper would be more accurate compared to Ref. [21], and the general variation trend has good consistency. The three-dimensional finite element model developed in this paper could effectively reflect various performances of ATEG, which would be an important foundation for analysis and optimization of Section 4.

4. Results and discussion

4.1. Analysis of twisted tape

As shown in Fig. 5, the control group is an ordinary ATEG and the experimental group is a TT-ATEG with a twisted tape in the heat exchanger. The parameters of the twisted tape in the experimental group are: $L = 0.097$ m, $R = 0.02$ m, $aa = 100$. The parameters of other part of structure set to the same and can be found in Table 2. The inlet temperature of waste gas T_h is 673 K and the inlet velocity V_h is 8.3814 m/s. To analyze the mechanism of increasing the twisted tapes to enhance the heat transfer performance, the results of the experimental group and the control group are conducted by Comsol, and analyzed in several perspectives as follows.

4.1.1. Analysis of flow rate and temperature

Fig. 6 (a) and (b) show the distribution of velocity vectors at the central section of the heat exchanger for the control and experimental groups. The velocity distribution in TT-ATEG is more irregular than that in ATEG. Under the influence of the twisted tape, the air fluid generates a swirling flow, and vortexes are produced near the wall. The fluids in the main flow region and the boundary layer are mixed with each other, which complicates the fluid flow. The above phenomenon shows that the twisted tape could effectively accelerate the heat transfer from the near-wall region to the mainstream area fluid, and the increase average flow velocity significantly, which improves the efficiency of heat transfer in TT-ATEG.

Fig. 6 (c) and (d) show the heat exchanger surface temperature distribution for the control and experimental groups. After adding the twisted tape, the average surface temperature of the heat exchanger increased from 494.25 K to 502.29 K, and the temperature increased by 8.04 K. Fig. 6 (e) and (f) shows the temperature distribution of the thermocouple in two groups. The average temperature of the hot end increased from 408 K to 420 K, indicating that in the state of high flow turbulence, the twisted tape greatly enhances fluid heat transfer inside the heat exchanger.

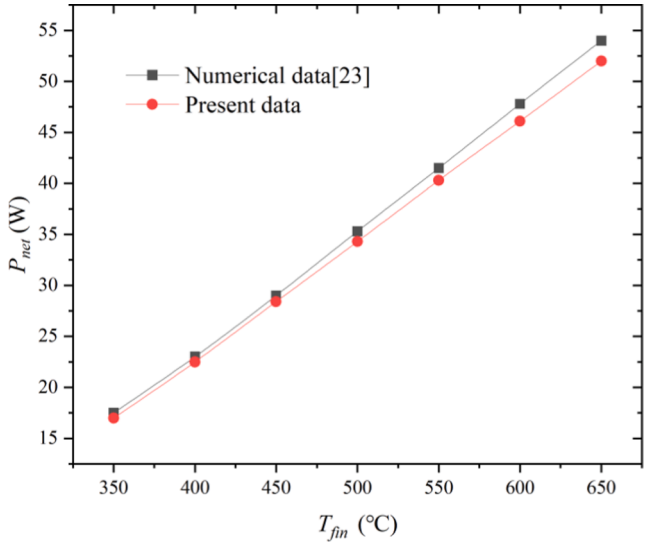

Fig. 4. Comparison of net power between present data and numerical data.

4.1.2. Analysis of heat transfer performance and friction loss

The twisted tape could also lead to a greater friction loss, which would increase the backpressure power loss of the engine and reduce the overall performance of the TT-ATEG. Nusselt number, *Nu*, and friction factor, *f*, are used to evaluate dual effects of heat transfer performance and friction loss.

The Fig. 7 shows the trend of Nusselt number *Nu* and friction factor *f* of the control group and the experimental group at different Reynolds numbers (6000–22000). The *Nu* of both groups increases linearly as *Re* increases, and the *Nu* of the experimental group is 33 %−60 % greater than the control group with the same *Re*, which indicated that the heat transfer performance of the experimental group is significantly better than control group. The friction coefficient *f* of the experimental group shows a significant decreasing trend with the increase of *Re*, while there is no discernible change in the control group. The *f* of the experimental group is 167 %–205 % greater than the control group, and the flow resistance in the pipe of the experimental group is significantly larger. The twisted tape increases the flow resistance of waste gas while improving the heat exchange performance. As far as TT-ATEG performance is concerned, the twisted tape would increase the output power P_{out} and also increase the backpressure power loss P_{loss}.

4.1.3. Analysis of electrical output performance

In order to further illustrate the problem intuitively, P_{net} and η are used to measure the output performance improvement of TT-ATEG.

Fig. 8(a) shows the trend of P_{out} and P_{loss} of the experimental group and the control group at different Reynolds numbers. The output power of the thermoelectric system in both groups increase with the increase of *Re*, and the P_{out} of the experimental group is significantly higher than the control group. After adding the twisted tape, the P_{loss} keeps increasing with the increase of *Re*, and the change trend becomes more and more obvious.

Fig. 8(b) shows the trend of P_{net} and η in the experimental group and the control group at different Reynolds numbers. The conversion efficiency η of both groups increases with the increase of *Re*. But the value of the experimental group is significantly larger, which shows that the twisted tape could improve the η at different *Re*. From the net power η perspective, it shows a trend of first increases and then decreases with the increase of *Re* in TT-ATEG, while it keeps increasing in ATEG.

When the Reynolds number is less than 12000, the twisted tape would bring both gain of P_{net} and η. The Reynolds number of air is closely related to the air flow rate.

4.2. Analysis of geometric parameters

Reasonable design of twisted tape could further improve the per-

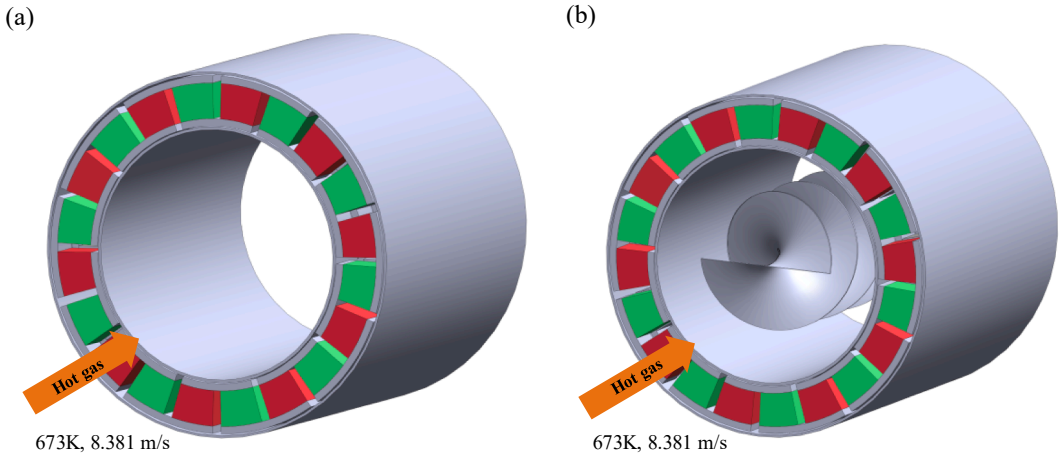

Fig. 5. Schematic diagram (a) control group (b) experimental group.

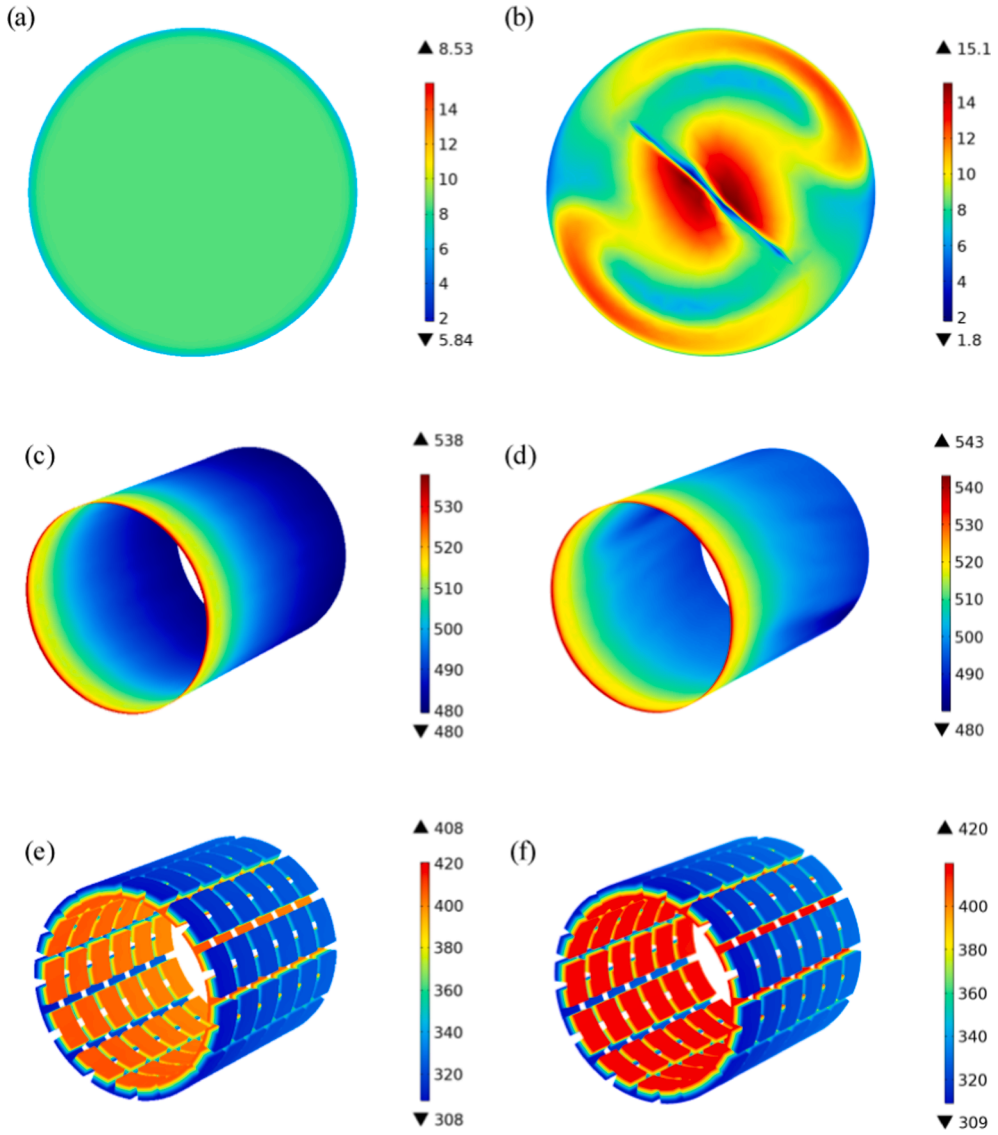

Fig. 6. Physical field performance distribution of Experimental and control groups. (a)(b) Velocity distribution at the central section of the heat exchanger; (c)(d) Temperature distribution of the heat exchanger surface; (e)(f) Temperature distribution of the thermocouple.

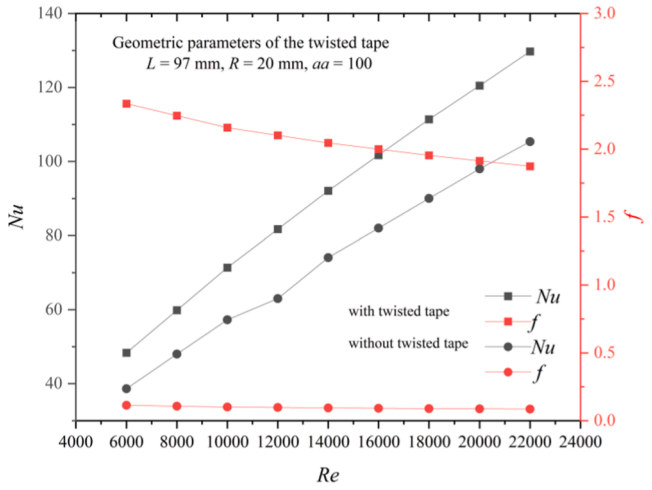

Fig. 7. Nusselt number and friction factor of experimental group and control group under different *Re*.

formance of TT-ATEG. In this section, we study the influence of the geometric parameters of the twisted tape (length *L*, radius *R*, twist ratio *aa*) on the thermoelectric performance. In order to quantify the influence of the gain generated by each parameter, J_{Pnet}, J_η is defined as the gain coefficient, which respectively denote the gain in net power and conversion efficiency of the experimental group compared to the initial control group.

$$J_{Pnet} = \left(\frac{P_{net}}{P_{net-ori}} - 1\right) \times 100\% \tag{24}$$

$$J_\eta = \left(\frac{\eta}{\eta_{ori}} - 1\right) \times 100\% \tag{25}$$

where P_{net},η denotes the net power and conversion efficiency of TT-ATEG. $P_{net\text{-}ori}$ and η_{ori} denote the net power and conversion efficiency of ATEG, because no twisted tape is added, changes in geometric parameters would not affect the values of the two. $P_{net\text{-}ori}$ and η_{ori} are 13.658 W and 3.571 %, respectively.

4.2.1. *Sensitivity study of length*

The trend of backpressure power loss P_{loss}, net power P_{net}, and net power gain J_{Pnet} with the length *L* of the twisted tapes is shown in Fig. 9 (a). The output power P_{out} is equal to the sum of net power P_{net} (green

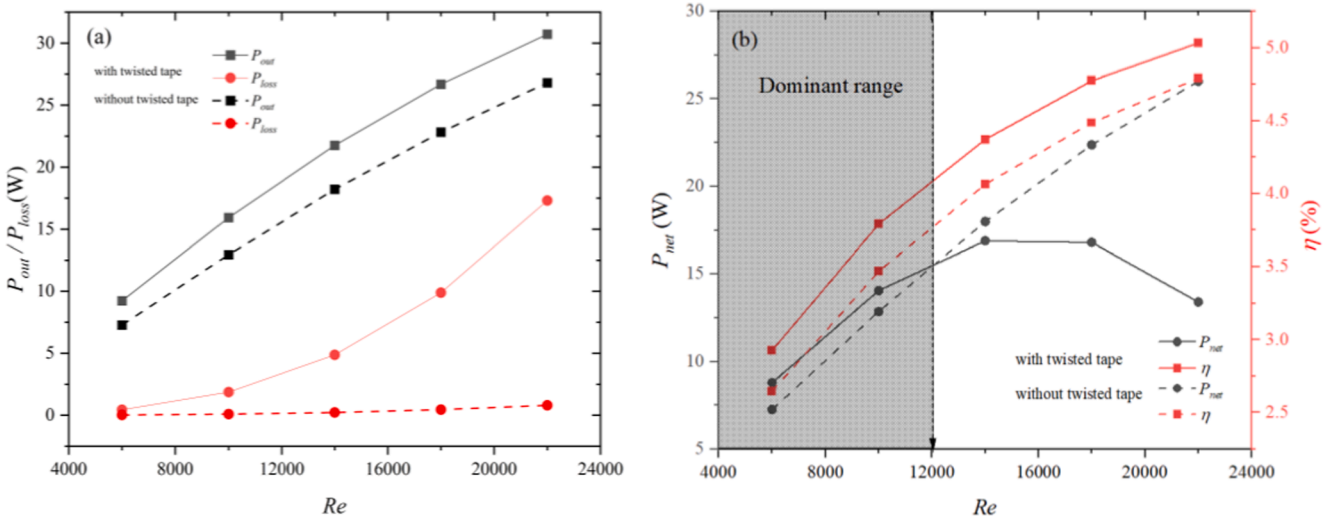

Fig. 8. Comparison of experimental group and control group (a) out power and backpressure power loss; (b) net power and conversion efficiency.

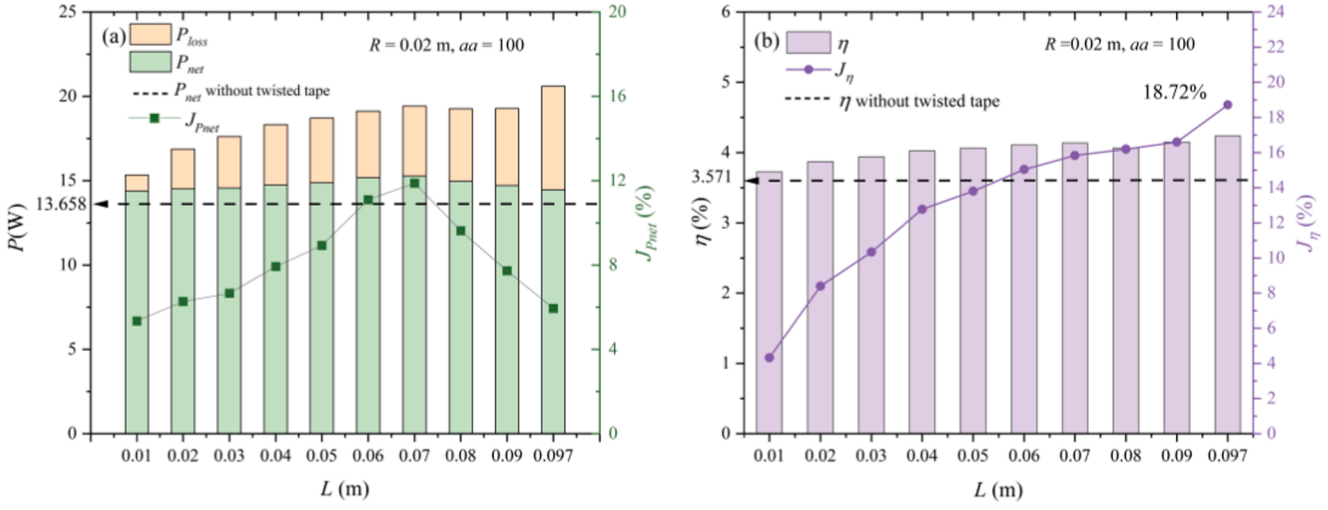

Fig. 9. Sensitivity study of different length of the twisted tape (a) Power and its gain (b) Efficiency and its gain.

part) and loss power P_{loss} (orange part) ($P_{out} = P_{net} + P_{loss}$). It shows that as the length of the twisted tape increases, the P_{out} and P_{loss} of the TT-ATEG are rising. The longer the length of the twisted tape, the greater the effect on the heat exchanger. Therefore, the temperature of the hot end increases and leading to a larger working temperature difference of ATEG. At the same time, the longer the twisted tape would bring greater backpressure power loss.

Overall, under different lengths of twisted tapes, the net power of TT-ATEG is higher than 13.658 W (dotted line) in the control group. The net power (green part) and net power gain (polyline) show a trend of increasing and then decreasing. When the length is 0.07, the P_{net} of the TT-ATEG can achieve a maximum value of 15.281 W and J_{Pnet} is 11.883 %.

The trend of conversion efficiency η (purple part) and conversion efficiency gain J_η (polyline) with respect to length is shown in Fig. 9(b). The η shows an increasing trend with the increase of length, and the η of TT-ATEG is always higher than that of the control group at different lengths. The maximum enhancement of conversion efficiency could reach at 18.72 %.

4.2.2. Sensitivity study of radius

The trend of backpressure power loss P_{loss}, net power P_{net}, and net power gain J_{Pnet} with respect to radius R of the twisted tapes is shown in Fig. 10(a). It can be seen that as the radius increases, both P_{out} and P_{loss} (orange part) show an upward trend. As the radius increases, the boundary layer becomes thinner, and the heat transfer performance and output power of TT-ATEG become better. At the same time, the larger the radius, the stronger the obstruction to the waste gas, so the greater the backpressure power loss.

The twisted tape may not always play a positive role in the improvement of the net power (green part). In Fig. 10(a), there is a critical point R_0, marking the radius when the output power gain brought by the twisted tape is 0 (J_{Pnet} is 0). When the radius is larger than R_0, the net power gain is negative, and vice versa.

The trend of conversion efficiency η (purple part) and conversion efficiency gain J_η (purple polyline) with respect to radius R is shown in Fig. 10(b). When the radius of twisted tape is taken as 0.01 m, the η (purple part) in both groups is very close, but as the radius increases, the conversion efficiency has been on an upward trend, and when the radius takes the maximum value, the η and J_η (purple polyline) reach the maximum value, which are 4.32 % and 21.064 % respectively.

4.2.3. Sensitivity study of twist ratio

Fig. 11(a) shows the trend of backpressure power loss P_{loss}, net power P_{net}, and net power gain J_{Pnet} with respect to the twist ratio *aa*. As the twist ratio increases, the P_{out} and P_{loss} (orange part) increase all the time. The larger the twist ratio is, the deeper the rotation of the twisted tape is. The distance between the streamlines of the exhaust is increased and the flow path becomes longer, the thermal contact area with the inner wall surface increases, and the heat exchange increases accordingly. It can be seen that the net power P_{net} (green part) has two extreme values with the increase of the twist ratio, which are obtained when the twist ratio is 50 and 125 respectively. It shows that an appropriate change interval can be selected for the twist ratio to avoid falling into local extreme values in the later optimization process. The P_{net} of TT-ATEG is always higher than that of ATEG under different twist ratios, but the overall gain of the net power J_{Pnet} is below 7 %.

Fig. 11(b) shows the trend of conversion efficiency η (purple part) and conversion efficiency gain J_η (polyline) with respect to twist ratio *aa*. The η has always been on the rise, which is greater than that of control group (3.571 %), and the maximum efficiency gain J_η (purple polyline) can reach 18.813 %, indicating that the twist ratio has a more obvious impact on the η.

4.3. Multi-objective joint optimization

The net power and efficiency of a thermoelectric power generation system are both important indicators to measure the system performance. However, it is difficult for the two to obtain their respective optimal values under the same geometric parameters. Configuring the weights reasonably of the two is the necessary means to achieve the optimal comprehensive performance of the system.

On this basis, the multi-objective optimization algorithm is used to complete the decoupling calculation of the key parameters (length, radius and torsion rate) of the twisted tape, and then realize the comprehensive energy efficiency improvement. Therefore, this part proposes a weighted method to establish a multi-objective function for the TT-ATEG module:

$$F = w \cdot \frac{\eta}{\eta_{opt}} + (1 - w) \cdot \frac{P_{net}}{P_{net-opt}} \tag{26}$$

where *w is* weight factor, η_{opt} and $P_{net\text{-}opt}$ represent the maximum value when optimizing with them as a single objective.

Also, in order to make the optimization results more generalized, it is necessary to define the dimensionless factors R_r and L_r (the twist ratio *aa* itself is a dimensionless factor, therefore there is no need to repeat the definition).

$$R_r = \frac{R}{R_{ex}} \tag{27}$$

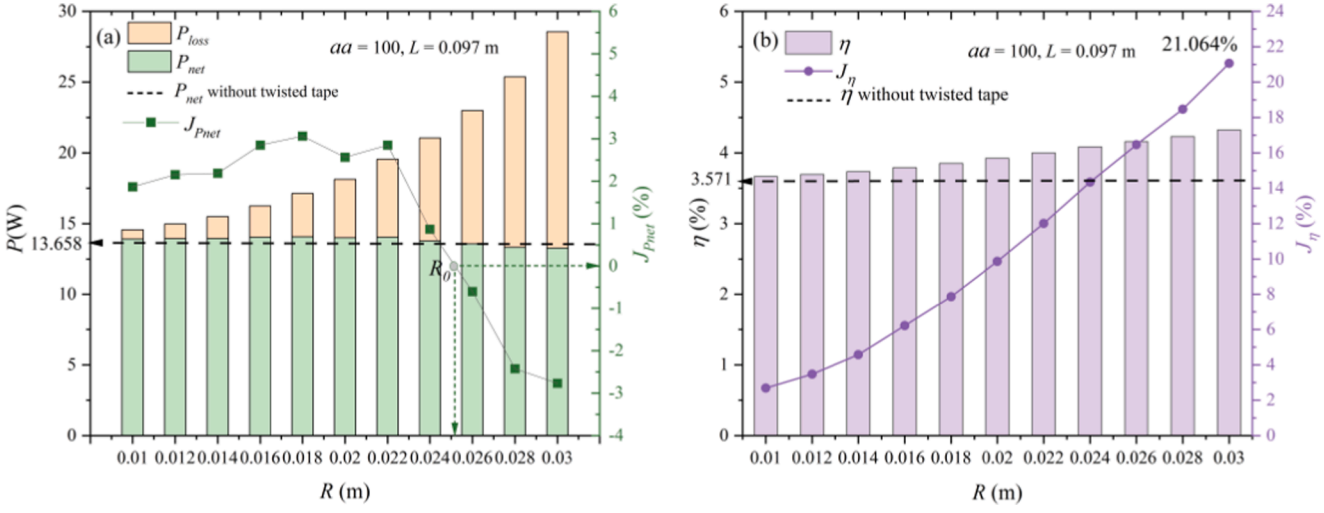

Fig. 10. Sensitivity study of various radius of the twisted tape (a) Power and its gain (b) Efficiency and its gain.

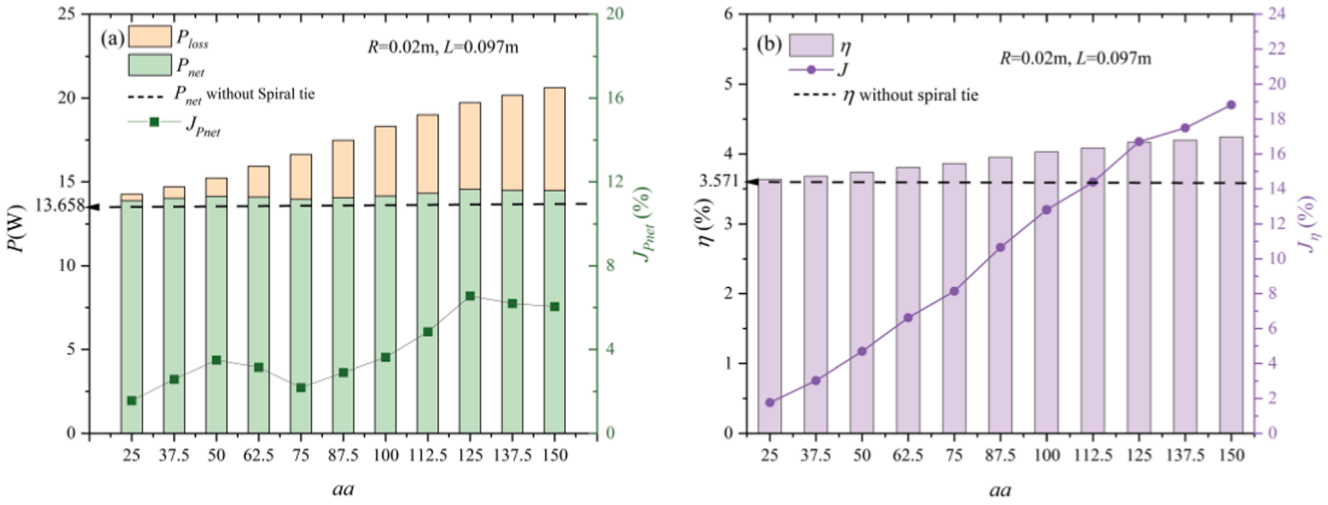

Fig. 11. Sensitivity study of various twist ratio (a) Power and its gain (b) Efficiency and its gain.

$$L_r = \frac{L}{L_{ex}} \tag{28}$$

R_r and L_r, respectively characterizing the radius ratio of the twisted tape (R) to hot-side heat exchanger (R_{ex}) and the length ratio of the twisted tape(L) to the hot-side heat exchanger (L_{ex}).

4.3.1. *Single objective optimization for P_{net} and η*

In order to comprehensively analyze the gain effect of the two indexes, the maximum value of which obtained by single objective optimization is used as the denominator of normalization processing.

In this part, the optimization is realized by calling the genetic algorithm toolbox in MATLAB.

Compared with the traditional optimization algorithm, the genetic algorithm is based on biological evolution, which has good convergence and requires less calculation time. The parameters of the algorithm are selected as follows: the initial population size is 10, the genetic termination algebra is 160, the selection operator adopts the roulette method, and the selection probability is 1/3; the crossover operator adopts the two-point crossover operator, and the crossover probability is 0.8; the mutation operator adopts Gaussian mutation, and the mutation probability is 0.05.

Fig. 12(a) shows the trend of net power and conversion power when the net power is used as the optimization objective function. After several iterations, the final net power is 15.278 W, and the conversion efficiency is 3.97 %. Compared with the control group, the optimization could increase the net power by 11.86 % and the efficiency by 12.57 %.

Fig. 12(b) shows the trend of net power and conversion power when conversion efficiency is the optimization objective function. After several iterations, the conversion efficiency is finally stabilized at 4.40 %, and the corresponding net power was 14.362 W. Compared with the control group, the net power is increased by 5.15 %, and the conversion efficiency is increased by 23.21 %.

For a clearer comparison of the two optimization results with the control group, Table 4 shows the results and the values of dimensionless factors. When single-objective optimization is carried out with net power and conversion efficiency respectively, the corresponding geometric parameters are different, and the degree of improvement of the two is also different.

4.3.2. *Multi-objective optimization for best performances*

According to the Eq. (26), a suitable weight factor should be found to get the best overall system performance. However, in the case of unknown weight factors, it is difficult to perform multi-objective optimization calculations. Therefore, this part first sets the weight with a step size of 0.1, and the values for multiple groups of net power and efficiency are shown in Table 5. At the same time, the gain function G represents the magnitude of simultaneous improvement of net power and conversion efficiency under multi-objective optimization, which is used to characterize the comprehensive performance of TT-ATEG.

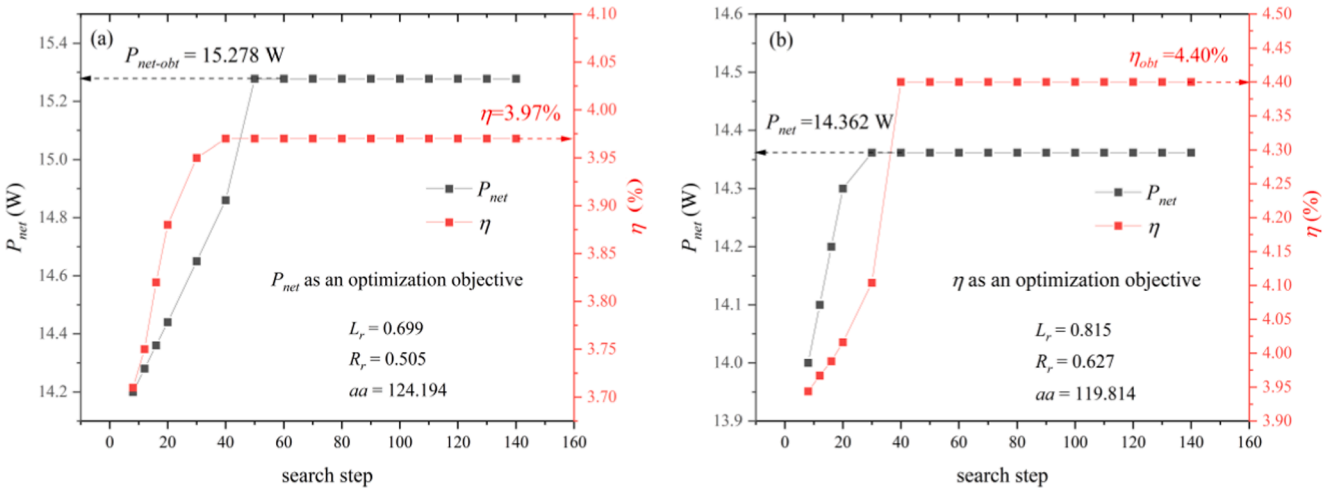

Fig. 12. Iterative trends of net power and conversion power (a) net power as the objective function; (b) conversion efficiency as the objective function.

Table 4
Optimal design with different objectives.

Group	P_{net}(W)	η(%)	J_{Pnet}(%)	J_{η}(%)	R_r(m)	L_r(m)	aa
Control group	13.658	3.571	/	/	/	/	/
P_{net} as object	15.278	3.97	11.86	12.57	0.699	0.505	124.194
η as object	14.362	4.40	5.15	23.21	0.815	0.627	119.814

Table 5
Objective function and geometric parameters under different w.

w	P_{net}(W)	η(%)	R_r(m)	L_r(m)	aa
0 (P_{net} as object)	15.278	3.967	0.505	0.699	124.194
0.1	15.128	3.993	0.651	0.799	79.701
0.2	14.376	4.219	0.668	0.754	136.568
0.3	14.518	4.208	0.708	0.841	86.352
0.4	14.879	4.021	0.757	1.000	50.000
0.5	14.98	4.120	0.473	1.000	50.000
0.6	14.766	4.079	0.508	0.942	74.221
0.7	14.919	4.198	0.722	0.593	95.766
0.8	15.08	4.375	0.714	0.479	136.840
0.9	14.769	4.236	0.659	0.928	117.478
1(η as object)	14.362	4.402	0.627	0.815	119.814

$$G_{all} = G_{Pnet} + G_{\eta} = \frac{P_{multi-obt}}{P_{obt}} + \frac{\eta_{multi-obt}}{\eta_{obt}} \tag{29}$$

where$P_{multi-obt}$,$\eta_{multi-obt}$,P_{obt} and η_{obt} represent the values of net power and efficiency under multi-objective optimization and single-objective optimization, respectively.

Table 5 shows the multi-objective optimization results under different weighting factors, including net power and conversion efficiency, as well as the corresponding geometric parameter values. It can be seen that when the value of w is 0 and 1, it represents the maximum weight of net power and efficiency, and the value of the weight factor can also reflect the relative importance of a single objective function. With the change of the w, the improvement of the two objective functions has its own emphasis. Fig. 13 shows the net power gain, efficiency gain, and total system gain under different weighting factors. When w is 0.8, the improvement effect is the most obvious. and G_{all} is the largest at 1.981, which is better than 1.901 and 1.940 under single-objective optimization. This verifies that multi-objective optimization is necessary and effective. At this point the values of the three dimensionless factors are taken as: $R_r = 0.714$, $L_r = 0.479$, $aa = 136.84$. It can be noticed that when the optimal result is obtained, the dimensionless factor L_r takes the minimum value, which shows that when the length ratio of the twisted tape and the heat exchanger is smaller, it is more helpful to improve the two thermoelectric performance indicators of net power P_{net} and efficiency η at the same time.

5. Conclusions

This article explores a simple and practical way to enhance the performance of ATEG. A novel TT-ATEG configured with a twisted tape is built to enhance the overall performance. The performance is analyzed based on fluid-thermal-electrical multiphysics model. The main conclusions are drawn as follows:

(1) A three-dimensional finite element model of TT-ATEG is established in Comsol for the first time. Twisted tape could increase output power of TT-ATEG but could also increase the frictional resistance and backpressure power loss.

(2) The radius, length and twist ratio of the twisted tape are the key factors that affect the efficiency of the TT-ATEG. The length and twist ratio will always make contribution to net power but radius is not, the net power first increases and then decreases as they increase.

(3) The optimum performance of TT-ATEG is obtained if the weight ratio of net power and conversion efficiency is 1:4. In such condition,

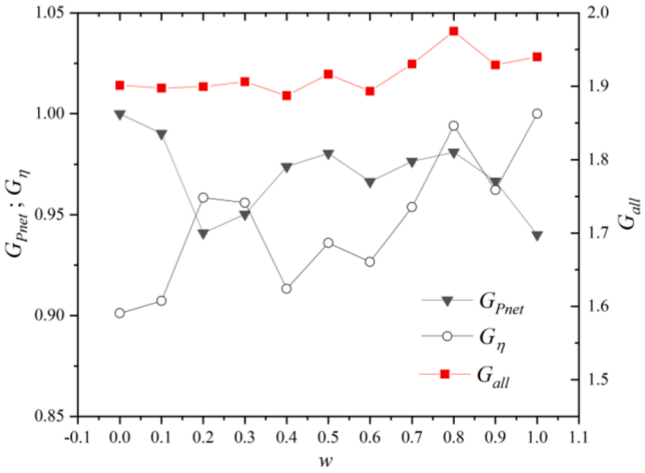

Fig. 13. Variations of G_{Pnet}, G_{η}, G_{all} under different w.

dimensionless factors radius ratio R_r and length ratio L_r and twist ratio of the twisted tape are 0.714, 0.479 and 136.84 respectively. Compared with the ATEG without twisted tape, the net power and efficiency are improved by 10.41 % and 22.51 %, respectively.

The results demonstrate that the novel design of TT-ATEG could accelerate the heat transfer effectively and enhance the overall performance.

CRediT authorship contribution statement

WenChao Zhu: Data curation, Investigation, Methodology, Writing – original draft. **Aoqi Xu:** Data curation, Writing – original draft. **Wenlong Yang:** Data curation, Software. **Binyu Xiong:** Investigation, Software, Writing – review & editing. **Changjun Xie:** Conceptualization, Funding acquisition, Project administration, Supervision, Writing – review & editing. **Yang Li:** Formal analysis, Methodology. **Lamei Xu:** Project administration, Validation. **Ying Shi:** Conceptualization. **Wei Lin:** Formal analysis, Validation.

Declaration of Competing Interest

The authors declare that they have no known competing financial interests or personal relationships that could have appeared to influence the work reported in this paper.

Data availability

Data will be made available on request.

Acknowledgments

This research was funded by the National Natural Science Foundation of China (51977164).

References

[1] Elghool A, Basrawi F, Ibrahim TK, Habib K, Ibrahim H, DMND I.. A review on heat sink for thermo-electric power generation: Classifications and parameters affecting performance. Energy Convers Manage 2017;134:260–77.

[2] Zhao Y, Wang S, Ge M, Li Y, Liang Z, Yang Y. Performance analysis of a thermoelectric generator applied to wet flue gas waste heat recovery. Appl Energy 2018;228:2080–9.

[3] Li X, Xie C, Quan S, Shi Y, Tang Z. Optimization of thermoelectric module's number and distribution pattern in an automotive exhaust thermoelectric generator. IEEE Access 2019;7:72143–57.

[4] Zhou S, Sammakia BG, White B, Borgesen P, Chen C. Multiscale modeling of Thermoelectric Generators for conversion performance enhancement. Int J Heat Mass Transf 2015;81:639–45.

[5] Zhu X, Cao L, Zhu W, Deng Y. 2. Enhanced interfacial adhesion and thermal stability in bismuth telluride/nickel/copper multilayer films with low electrical contact resistance. Adv Mater Interfaces 2018;5(23):1801279.

[6] Huang S, Xu X. A regenerative concept for thermoelectric power generation. Appl Energy 2017;185:119–25.

[7] Kempf N, Zhang Y. Design and optimization of automotive thermoelectric generators for maximum fuel efficiency improvement. Energy Convers Manage 2016;121:224–31.

[8] Zhang J, Wu Di, He D, Feng D, Yin M, Qin X, et al. Extraordinary thermoelectric performance realized in n-type PbTe through multiphase nanostructure engineering. Adv Mater 2017;29(39):1703148.

[9] Perumal S, Samanta M, Ghosh T, Shenoy US, Bohra AK, Bhattacharya S, et al. Realization of high thermoelectric figure of merit in GeTe by complementary Co-doping of Bi and In. Joule 2019;3:2565–80.

[10] Zhao J, Xu W, Kuang Z, Long R, Liu Z, Liu W. Segmental material design in thermoelectric devices to boost heat-to-electricity performance. Energy Convers Manage 2021;247:114754.

[11] Shittu S, Li G, Xuan Q, Zhao X, Ma X, Cui Yu. Electrical and mechanical analysis of a segmented solar thermoelectric generator under non-uniform heat flux. Energy 2020;199:117433.

[12] Meng F, Chen L, Sun F. Performance analysis for two-stage TEC system driven by two-stage TEG obeying Newton's heat transfer law. Math Comput Modell 2010;52 (3-4):586–95.

[13] Asaadi S, Khalilarya S, Jafarmadar S. A thermodynamic and exergoeconomic numerical study of two-stage annular thermoelectric generator. Appl Therm Eng 2019;156:371–81.

[14] Wang Y, Li S, Zhang Y, Yang X, Deng Y, Su C. The influence of inner topology of exhaust heat exchanger and thermoelectric module distribution on the performance of automotive thermoelectric generator. Energy Convers Manage 2016;126:266–77.

[15] Li B, Huang K, Yan Y, Li Y, Twaha S, Zhu J. Heat transfer enhancement of a modularised thermoelectric power generator for passenger vehicles. Appl Energy 2017;205:868–79.

[16] Luo D, Wang R, Yu W, Sun Z, Meng X. Modelling and simulation study of a converging thermoelectric generator for engine waste heat recovery. Appl Therm Eng 2019;153:837–47.

[17] Yang W, Zhu WenChao, Li Y, Zhang L, Zhao Bo, Xie C, et al. Annular thermoelectric generator performance optimization analysis based on concentric annular heat exchanger. Energy 2022;239:122127.

[18] Wang T, Luan W, Wang W, Tu S. Waste heat recovery through plate heat exchanger based thermoelectric generator system. Appl Energy 2014;136:860–5.

[19] Kim TY, Lee S, Lee J. Fabrication of thermoelectric modules and heat transfer analysis on internal plate fin structures of a thermoelectric generator. Energy Convers Manage 2016;124:470–9.

[20] Lu X, Yu X, Qu Z, Wang Q, Ma T. Experimental investigation on thermoelectric generator with non-uniform hot-side heat exchanger for waste heat recovery. Energy Convers Manage 2017;150:403–14.

[21] Niu ZQ, Diao H, Yu SH, Jiao K, Du Q, Shu GQ. Investigation and design optimization of exhaust-based thermoelectric generator system for internal combustion engine. Energy Convers Manage 2014;85:85–101.

[22] Borcuch M, Musiał M, Gumuła S, Sztekler K, Wojciechowski K. Analysis of the fins geometry of a hot-side heat exchanger on the performance parameters of a thermoelectric generation system. Appl Therm Eng 2017;127:1355–63.

[23] Yang Y, Wang S, Zhu Yu. Evaluation method for assessing heat transfer enhancement effect on performance improvement of thermoelectric generator systems. Appl Energy 2020;263:114688.

[24] Shen Z, Wu S, Xiao L. Theoretical analysis on the performance of annular thermoelectric couple. Energy Convers Manage 2015;89:244–50.

[25] Zhang M, Wang J, Tian Y, Zhou Y, Zhang J, Xie H, et al. Performance comparison of annular and flat-plate thermoelectric generators for cylindrical hot source. Energy Rep 2021;7:413–20.

[26] Jia Y, Zhang Z, Wang C, Sun H, Zhang W. Design and parameter study of a thermoelectric generator for waste heat recycling in flexible micro-light-emitting diodes. Appl Therm Eng 2022;200:117568.

[27] Cao Y, Abu-Hamdeh NH, Moria H, Asaadi S, Alsulami R, Sadighi Dizaji H. 4. A novel proposed flexible thin-film solar annular thermoelectric generator. Appl Therm Eng 2021;183:116245.

[28] Ge M, Wang X, Zhao Y, Wang S, Liu L. Performance analysis of vaporizer tube with thermoelectric generator applied to cold energy recovery of liquefied natural gas. Energy Convers Manage 2019;200:112112.

[29] Piriyarungrod N, Eiamsa-Ard S, Thianpong C, Pimsarn M, Nanan K. Heat transfer enhancement by tapered twisted tape inserts. Chem Eng Process 2015;96:62–71.

[30] Noorbakhsh M, Ajarostaghi SSM, Zaboli M, Kiani B. Thermal analysis of nanofluids flow in a double pipe heat exchanger with twisted tapes insert in both sides. J Therm Anal Calorim 2022;147(5):3965–76.

[31] Mashayekhi R, Eisapour AH, Eisapour M, Talebizadehsardari P, Rahbari A. Hydrothermal performance of twisted elliptical tube equipped with twisted tape insert. Int J Therm Sci 2022;172:107233.

[32] Luo D, Wang R, Yu W, Sun Z, Meng X. Theoretical analysis of energy recovery potential for different types of conventional vehicles with a thermoelectric generator. Energy Procedia 2019;158:142–7.

[33] Wan Q, Liu X, Gu B, Bai W, Su C, and Deng Y. Thermal and acoustic performance of an integrated automotive thermoelectric generation system. Appl Therm Eng 2019; 158: 113802.

[34] Luo D, Sun Z, Wang R. Performance investigation of a thermoelectric generator system applied in automobile exhaust waste heat recovery. Energy 2022;238: 121816.

[35] Zakaria L, Sakina E-H, Abdelaziz B, Karim L, Bara E-H. Numerical study of the turbulent natural convection of nanofluids in a partially heated cubic cavity. Therm Sci 2021;25:57.

[36] Fan S, Gao Y. Numerical simulation on thermoelectric and mechanical performance of annular thermoelectric generator. Energy 2018;150:38–48.

[37] Luo D, Wang R, Yu W. Comparison and parametric study of two theoretical modeling approaches based on an air-to-water thermoelectric generator system. J Power Sources 2019;439:227069.

[38] Hu W, Li X, Wang J, Tian Z, Zhou B, Wu J, et al. Experimental research on the convective heat transfer coefficient of photovoltaic panel. Renewable Energy 2022; 185:820–6.

[39] He W, Wang S, Li Y, Zhao Y. Structural size optimization on an exhaust exchanger based on the fluid heat transfer and flow resistance characteristics applied to an automotive thermoelectric generator. Energy Convers Manage 2016;129:240–9.

[40] Liakopoulos A, Sofos F, Karakasidis TE. Darcy-Weisbach friction factor at the nanoscale: From atomistic calculations to continuum models. Phys Fluids 2017;29 (5):052003.

[41] Lesage FJ, Sempels ÉV, Lalande-Bertrand N. A study on heat transfer enhancement using flow channel inserts for thermoelectric power generation. Energy Convers Manage 2013;75:532–41.